Supplementary Information for the paper

Topological Fano Resonances

Farzad Zangeneh-Nejad and Romain Fleury*

Laboratory of Wave Engineering, School of Electrical Engineering, EPFL, Station 11, 1015 Lausanne, Switzerland

**To whom correspondence should be addressed. Email: romain.fleury@epfl.ch*

This supplementary information contains the following sections:

I. Symmetry-protected bound states in the continuum (BICs)

We provide here an analysis of the bound states coexisting in the radiation continuum of the proposed acoustic waveguide. Consider the two dimensional acoustic parallel-plate waveguide represented in Fig. S1a. Assume first that the waveguide does not contain any obstructing cylinder. The corresponding eigenmodes are either even or odd with respect to the dashed green line due to vertical inversion symmetry. Solving the scalar Helmholtz equation with the Neumann boundary condition being applied to the walls of the waveguide, one can easily find that the even modes do not have a cutoff frequency, whereas the odd modes possess a cutoff frequency of $f_c = \pi c_s/2h$ (c_s is the speed of sound). Next suppose a single cylindrical obstacle is embedded inside the waveguide, whose center is placed right at the centerline. In this case, since the obstacle preserves the vertical mirror symmetry, the entire structure remains mirror-symmetric and the resulting eigenstates will still be either even or odd. An odd mode localized to the obstructing cylinder, and below the cutoff frequency of the radiation odd waves, i.e. f_c, can then coexist within the continuum of the even modes, while it remains completely decoupled from them because of its different symmetry [1]. Shown in Fig. S1b is the field profile of this mode. Based on its profile distribution, one can deduce that it is not possible for the even (radiation) modes traveling from one side to the other side of the waveguide to excite this odd-symmetric state, because of the different symmetry. Consequently, this mode is a symmetry-protected bound-state in the continuum (BIC): it is completely hidden in the transmission or absorption spectra when carrying out a scattering experiment [1].

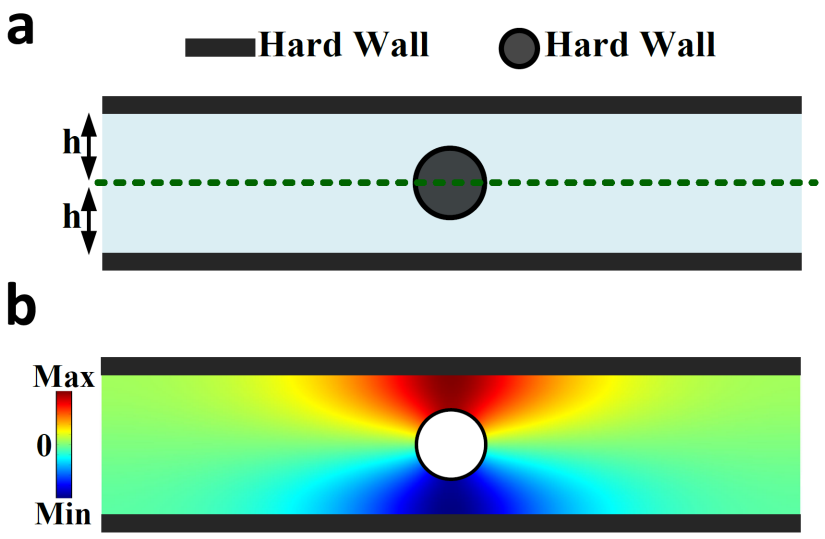

Fig. S1: Symmetry-protected bound states in the continuum in an acoustic waveguide. a, An acoustic waveguide containing an obstructing cylinders is considered. The waveguide supports a continuum of radiation modes possessing even symmetry with respect to the dashed green line. **b,** An odd mode localized to the obstructing cylinder, and below the cutoff frequency of $\frac{\pi c_s}{2h}$ can happen to coexist within the radiation continuum of the waveguide while remaining perfectly bounded to the obstacle due to its different symmetry.

II. Scaling property of the radiative (even) and BIC (odd) modes

This section reports on the effect of scaling lattice constant on the band structure of the crystal shown in Fig. 2a. As discussed in the article, the even eigenmodes (marked with blue colors in the dispersion diagram) exhibit a frequency dispersion resembling that of a typical sonic crystal. Hence, once the lattice constant is increased (or decreased), their dispersion bands move to lower (or higher) frequencies. On the contrary, scaling the lattice constant will not significantly affect the frequency position of the odd (BIC) mode due to the fact that it is mainly due to a resonance in the vertical direction [2,3]. This expectation is confirmed by gradually increasing the lattice constant and calculating the corresponding band structures in Fig. S2. Inspecting the results of this figure reveals that the position of the BIC mode (the red band) is negligibly affected by the scaling (only its group velocity changes due to a change of the evanescent coupling constant

between the BICs, which is proportional to the overlap integral between adjacent BIC modes), whereas the bands associated with the even modes are moved towards lower frequencies.

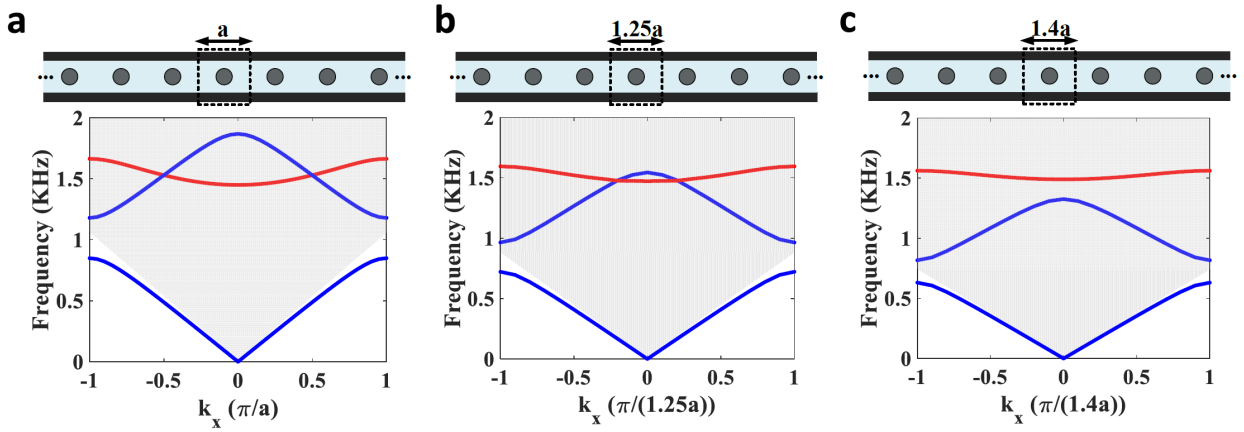

Fig. S2: Effect of scaling the lattice constant on the band structure of the system under study. **a,** Band structure of the system when the lattice constant is assumed to be *a=16.3 cm*. The waveguide continuum is marked with the grey area, **b,c**, Same as panel a except that the lattice constant is increased to *1.2a* and *1.4a*, respectively. The blue dispersion bands corresponding to the even eigenstates are moved to the lower frequency range, whereas the position of the red band associated with the BIC mode is not affected.

III. Zak phase calculation

This section provides supplementary details regarding the calculation of the Zak phases of the bands. We start with the standard equation for the Berry connection in one dimension [4]

$$A(k) = \langle \psi | i \partial_k | \psi \rangle dk \tag{S1}$$

where ψ is the eigenstate of the system and k is the Bloch wavenumber. The Zak phase of each band can then be calculated by integrating the Berry connection over the whole Brillouin zone as

$$\gamma = \int_{BZ} A(k) \tag{S2}$$

To provide more insight into the calculation process, we represent the Berry connection and Zak phases of the dispersion bands for the non-trivial crystal of Fig. 2d. To this end, for each band,

we separately calculate the expression of Eq. S1 for all k, making use of the mode profiles of their corresponding eigenstates.

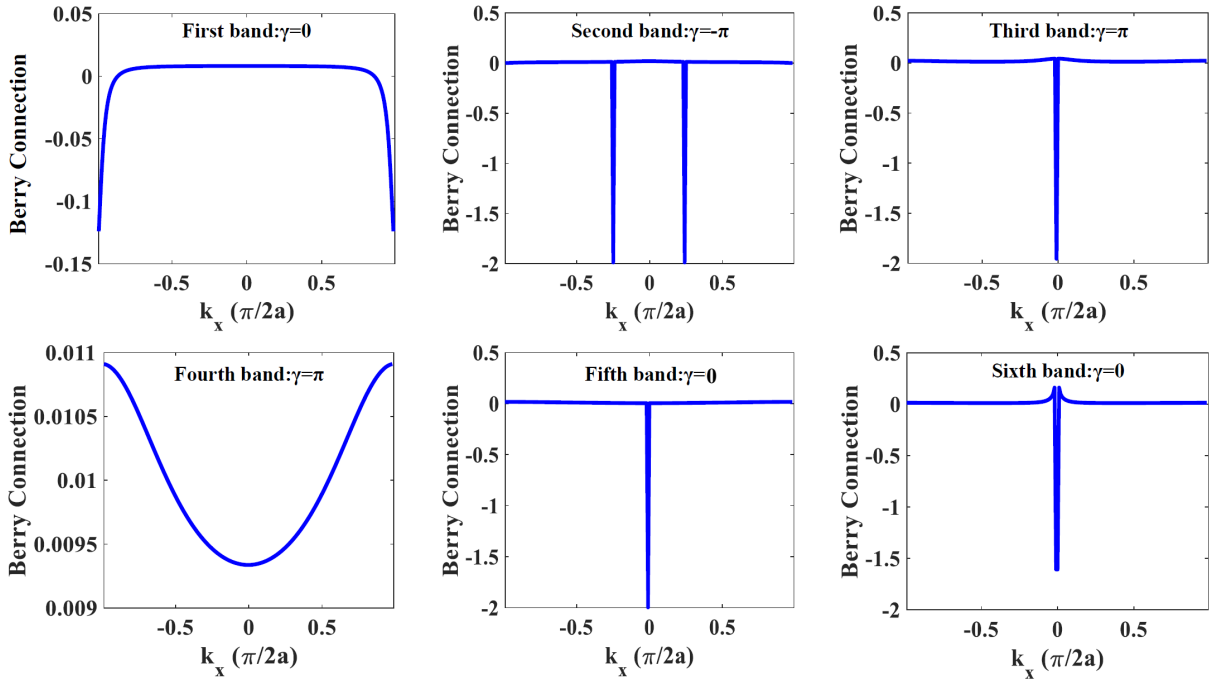

Fig. S3: Zak phase calculation of the bands for the non-trivial acoustic system. The figure shows the Berry connections associated with the bands obtained in Fig. 2d. Integrating the Berry connections over the whole Brillouin zone gives the Zak phase of the band of interest.

Fig. S3 reports the resulting Berry connections for all of the six bands under investigation. The summation over all values of $A(k)$ leads to the Zak phases of $\gamma_1 = 0$, $\gamma_2 = -\pi, \gamma_3 = \pi$, $\gamma_4 = \pi$, $\gamma_5 = 0$, $\gamma_6 = 0$ for the first to sixth bands, respectively. Employing a similar procedure, one obtains Zak phases of zero for all six bands of the trivial system. These observations resemble the topological phases emerging in the so-called Su-Schrieffer–Heeger (SSH) chain with detuned intercell and intracell coupling coefficients [4], although a tight-binding SSH model is only valid here for the BIC (odd) bands (a plane-wave expansion model is more suited to describe the even bands). We have also checked, by performing similar calculations on a system with all resonators

shifted up from the centerline of the waveguide, that such a motion does not change the topological classification of the bands.

IV. Field profile of the edge states of the proposed topological system

This section provides the field profiles of the edge states forming at the interface between the two insulators in Fig. 3a. As mentioned in the main article, the corresponding edge states can be divided into two different groups according to their symmetry. The first group comprises the even edge states. Shown in Fig. S4a is the field profile of such edge states. The second group includes the odd edge state, originating from the coupled BICs shown in Fig. S1b. The field profile of this edge state is shown in Fig. S4b. It should be noted that while both types of edge states are highly localized to the interface, they offer different resonance linewidth when coupled to an external plane wave in a finite system. More specifically, since the odd edge mode is perfectly decoupled from the radiation waves due to its different symmetry, it provides a resonance with zero radiative linewidth (i.e. an infinite quality factor, in the ideal lossless case). The even edge mode, however, leaks out to the radiation continuum, leading to a finite quality factor or a non-zero radiative linewidth (complex resonance frequency).

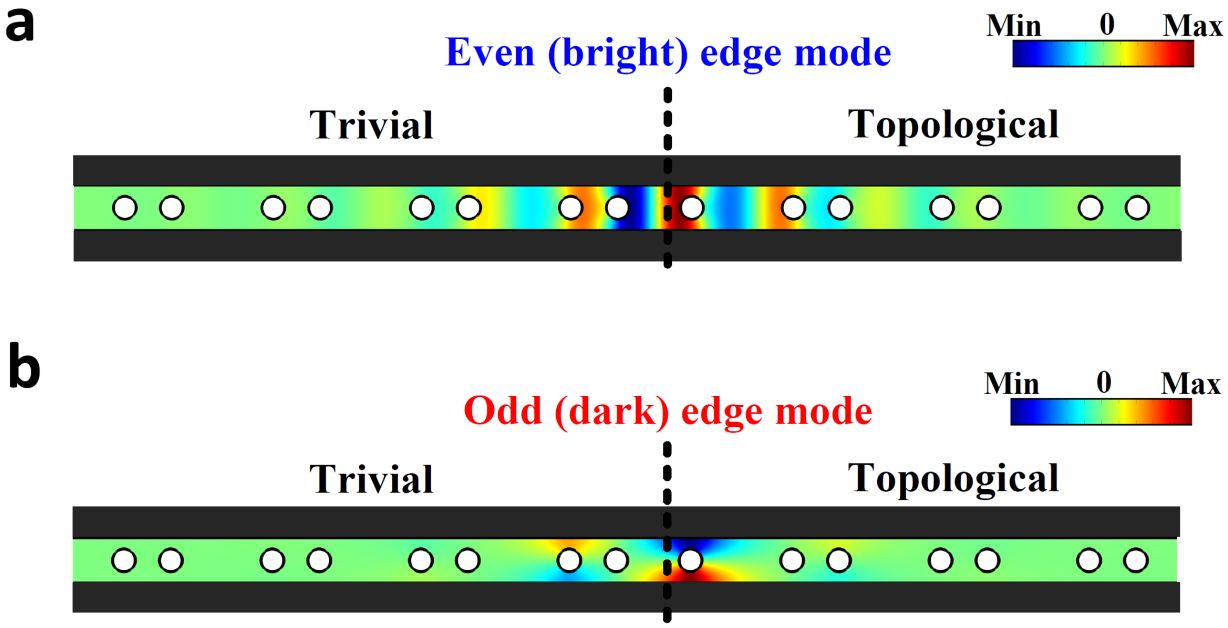

Fig. S4: Field profile of the edge states formed at the interface between the two insulators. **a,** Field profile of the even edge mode originating from the radiation modes, **b,** Field profile of the odd edge mode stemming from the BIC mode. Although both even and odd edge modes are bounded to the interface, only the even edge mode offers a finite resonance linewidth as the odd edge mode is completely decoupled from the radiation continuum due to its different symmetry.

V. Topological Fano resonances for electromagnetic (EM) waves

In this section, we demonstrate how topological Fano resonances can be obtained for electromagnetic waves. Consider a microwave parallel plate waveguide with the palate separation of *2h* (Fig. S5a). Since the waveguide is infinite in the out-of-plane direction, the solution to Maxwell equations can be decomposed into transverse electric (TE) and transverse magnetic (TM) parts. Here, without loss of generality, we investigate the TE part and assume that the electric field is polarized along z (out of plane direction). Solving the corresponding equations for the E_z component of the field with Dirichlet boundary conditions being applied to the waveguide plates, one can easily find that the resulting eigenmodes (E_z) are required to be even with respect to the centerline, and have a cutoff frequency of $f_c = \pi c/2h$ (c is the speed of light).

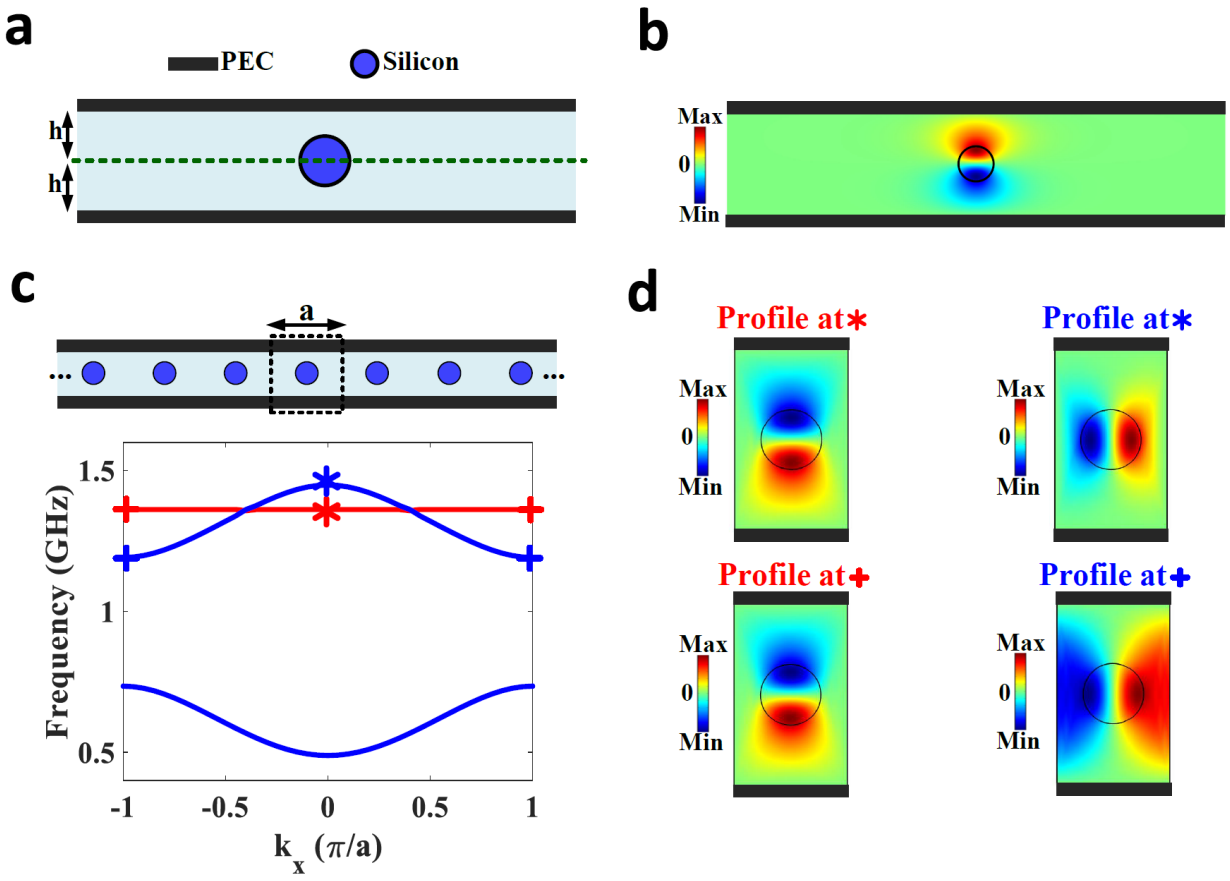

Fig. S5: Inducing independent topological subspaces in a microwave waveguide. **a,** A microwave parallel plate waveguide containing a single silicon rod placed on the centerline is considered. **b,** Profile of the corresponding bound state forming within the radiation continuum of the waveguide**. c,** We consider a periodic lattice of silicon rods inside the waveguide. The BIC (odd) mode has a low-dispersive behavior (the red band), while the radiation (even) modes exhibit a stronger frequency dispersion (blue bands). **d,** Profile of the even and odd eigenstates at certain Bloch wavenumbers.

Suppose now a circular dielectric obstacle (a silicon rod) is placed right at the centerline. The dielectric rod supports a set of resonances whose E_z components can be even or odd with respect to the centerline. If the resonance frequency of one of the odd dielectric modes falls above the waveguide cutoff (f_c), it can coexist in the radiation continuum of the even waveguide modes, while, simultaneously, remaining perfectly bounded to the rod due to its different symmetry [5,6]. Fig. S5b (second panel) depicts the profile (E_z component) of the corresponding BIC mode

obtained via FEM simulations. Now that we successfully realized a bound state in the radiation continuum of the waveguide, we pursue the same procedure as the acoustic case to achieve a topological Fano resonance. We first form a periodic lattice of the dielectric obstacles and calculate its dispersion (Fig. S5c). The dispersion bands are colored according to the symmetry of their eigenmodes represented in Fig. S5d. We further note that, similar to the acoustic case, one can adjust the frequency of the radiation (even) modes by scaling the lattice constant, whereas the position of the dispersion band of the BIC (odd) mode is not affected by scaling.

Consider now the configuration of Fig. S6a, where different topological phases are induced by detuning the intercell and intracell couplings between the dielectric resonators. The profiles of the corresponding even and odd edge modes are shown in the second and third panel, respectively. By subtly choosing the lattice constant, we have made the odd edge mode coexist within the spectral range of the even one. The scattering experiment (Fig. 6a, bottom panel, dashed red spectrum), however, reveals only the presence of the even edge mode since the odd edge mode is decoupled from even-symmetric waves. By slightly moving the dielectric resonators from the centerline, however, a topological Fano resonance emerges as a result of the small leakage of the odd edge mode to the radiation waves (the solid blue line). Just like in acoustics, the obtained Fano resonance is expected to be robust against disorder. To assess this robustness, we have randomly changed the position of the resonators to achieve the largely disordered configuration of Fig. S6b (first panel, average shift is 4.6% of h, with no preferred direction). Shown in the second and third panels are the profiles of the corresponding even and odd edge modes, respectively. Notably, the resonance frequencies of both bright and dark resonances can shift but no Anderson localization occurs. The resulting Fano lineshape is

therefore expected to be preserved. This is indeed evident from the transmission spectrum of the waveguide in the fourth panel, confirming the high robustness of the topological Fano resonance.

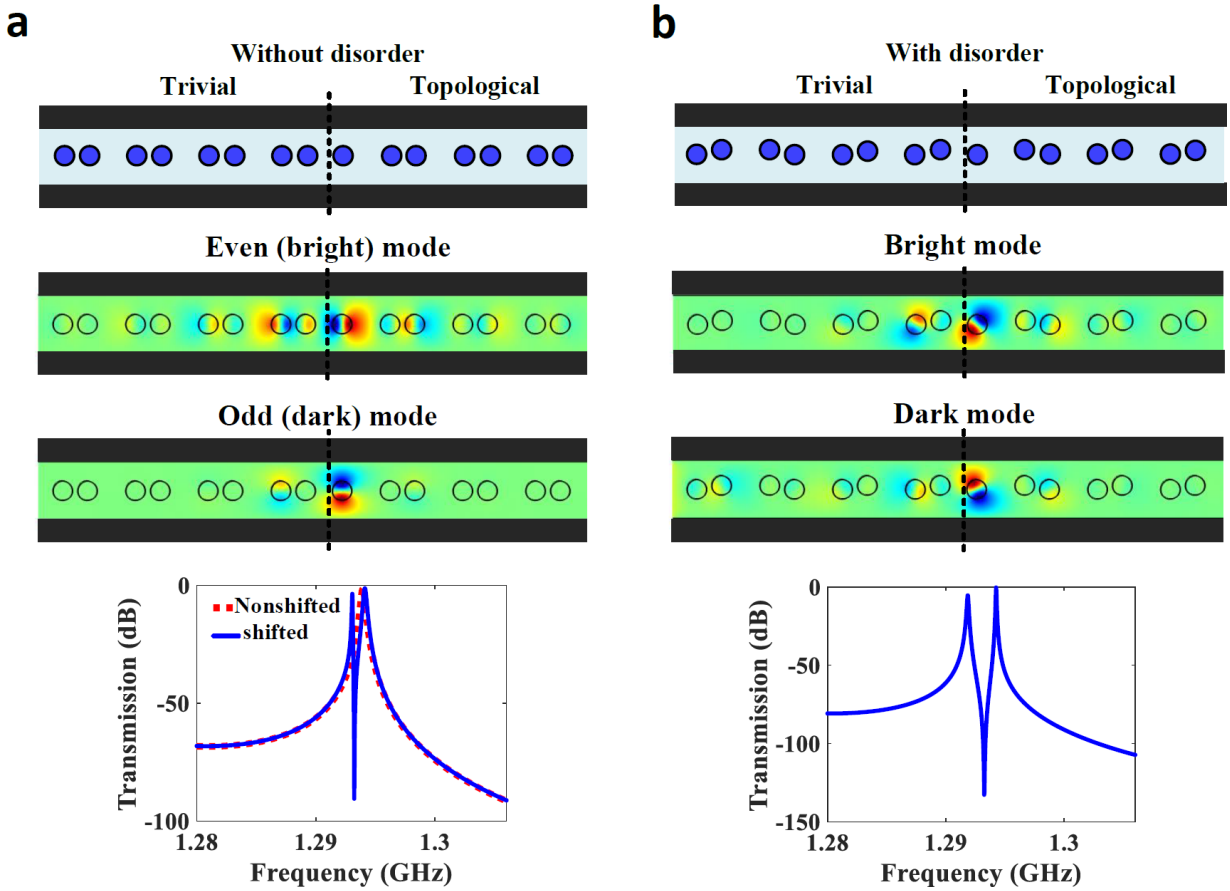

Fig. S6: Electromagnetic topological Fano resonances a, Ideal case without position disorder, for a system of dielectric rods in a parallel plate waveguide. A topological Fano resonance is observed. **b,** Same as panel a) but for in the presence of position disorder. The presence and shape of the Fano resonance is protected against disorder by the topology of the bulk insulators.

VI. Effect of horizontal and vertical disorder on the topological Fano resonance

This section compares the effect of disorder in right/left direction on the topological Fano resonance with that of up/down direction in the case of the acoustic system. As mentioned in the main text, no preferred direction was considered in the random realization of disorder imparted to the sample. Here we report the different effect of horizontal versus vertical

disorder. As it is seen in Fig. S7, disorder in left/right direction affects more strongly the shape of the Fano resonance than the same level of disorder imparted in the up/down direction. While vertical shifts mostly affect the frequency of the odd BIC modes (eigen-frequencies of the tight-binding BIC chain), horizontal shifts change both the distance between two scattering crystal planes (affecting the even modes), and the overlap integrals between adjacent BIC modes. Therefore, the effect of horizontal position disorder on the Fano shape is larger because it affects both of the bright and dark modes. The main point, however, is that, regardless of the direction in which the disorder is applied, the Fano line shape will be present, and not be polluted by the occurrence of spurious disorder-induced peaks as long as the disorder does not close the surrounding topological band-gaps (which happens only for very large disorder levels, like for any topological insulator, as a consequence of Anderson localization).

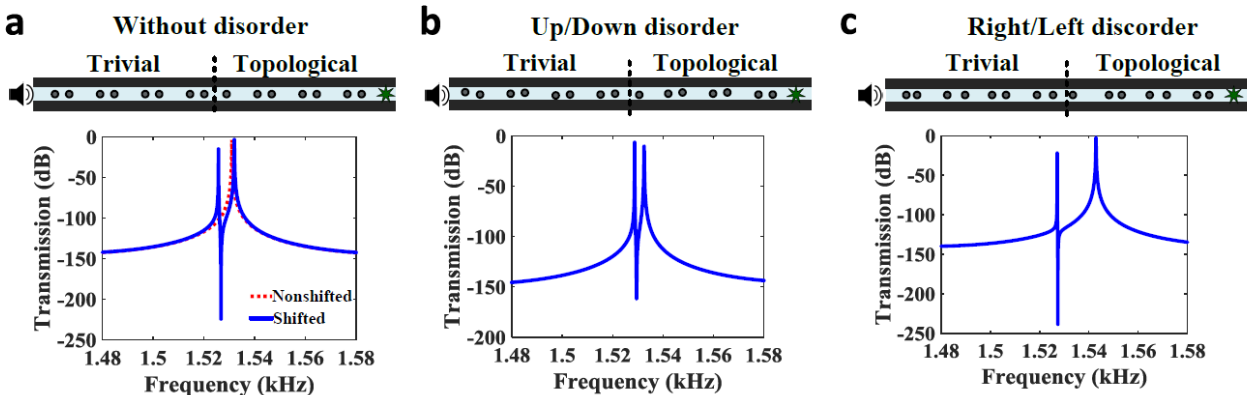

Fig. S7: Comparison between left/ right and up/down types of disorder, a, Original sample without disorder, **b,** Effect of position disorder along the perpendicular direction. **c,** Effect of position disorder along the waveguide direction.

VII. Numerical methods

Full-wave finite-element simulations were performed using Comsol Multiphysics (Acoustic and RF modules). For the band structure analysis, we first considered a single unit cell of the crystal and meshed it. We then applied Floquet and Dirichlet boundary conditions to the sides of the simulation domain. Dispersion curves were then conveniently extracted using an eigenfrequency solver by varying the Floquet-Bloch wavenumber in the first Brillouin zone. The corresponding eigenmodes were then used to compute the Zak phases of the bands. In the scattering numerical experiment, we excite the waveguide from the left side with a time-harmonic incident plane-wave with unit amplitude, using radiation-free boundary conditions with a plane-wave incident field. We then measured the amount of pressure at the transmission side of the waveguide to obtain the transmission coefficient.

VIII. Experimental methods

An acrylic extruded clear square tube was used as the acoustic waveguide (49 cm^2 internal cross-section). Nylon 6 continuous cast black rods were then manually embedded within the waveguide to implement the topological chain under study. The overall sample was then put in the setup shown in Fig. S8. The setup comprises a loudspeaker connected to a Bruel&Kjaer 2706 amplifier in order to maximize the signal to noise ratio (SNR), three ICP® microphones measuring the sound pressure at different points of the waveguide, a home-built anechoic termination made of melamine foam connected to the end of the waveguide, and a Data Physics Quattro signal analyzer connected to a computer. To obtain the transmission (or reflection) coefficient of the sample, we excite the waveguide with a burst noise signal, measure the amount of pressures P_1, P_2, and P_3 and use the following equations:

$$R = \frac{H_{12}e^{-j\beta z_2} - \mathrm{e}^{-j\beta z_1}}{\mathrm{e}^{j\beta z_1} - H_{12}e^{-j\beta z_2}}$$
$$T = \frac{H_{32}(\mathrm{e}^{-j\beta z_2} + \mathrm{R}\mathrm{e}^{j\beta z_2})}{\mathrm{e}^{-j\beta z_3}} \quad \text{(S3)}$$

where $\beta = \frac{2\pi f}{c_s}$ is the propagation constant, z_1, z_2, and z_3 correspond to the position of the microphones and H_{12} and H_{32} are the transfer functions defined by

$$H_{12} = \frac{P_1}{P_2}$$
$$H_{32} = \frac{P_3}{P_2} \quad \text{(S4)}$$

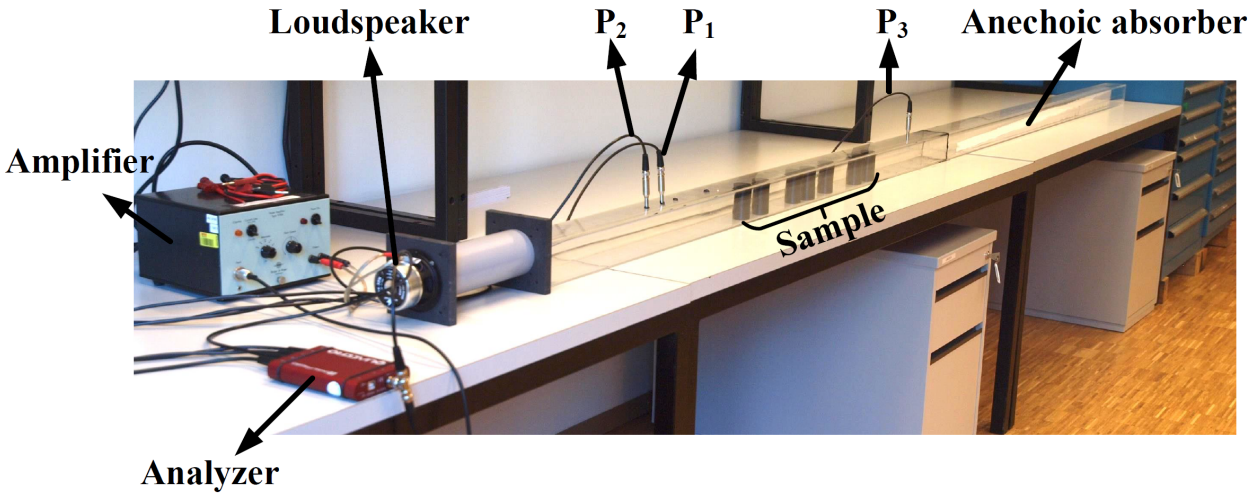

Fig. S8: Experimental setup used to observe topological Fano resonances. The setup consists of three ICP® microphones, an anechoic acoustic absorber connected to the end of the waveguide, a loudspeaker, a power amplifier and a Data Physics Quattro data analyzer controlled by a computer.

IX. Supplementary references

1. C. W. Hsu, B. Zhen, A. D. Stone, J. D. Joannopoulos, and M. Soljacic, Nat. Rev. Mater. **1**, (2016).
2. S. Yves, R. Fleury, F. Lemoult, M. Fink, and G. Lerosey, New J. Phys. 19, (2017).

3. S. Yves, R. Fleury, T. Berthelot, M. Fink, F. Lemoult, and G. Lerosey, Nat. Commun. 8, (2017).
4. Asbóth, János K., László Oroszlány, and András Pályi. "A Short Course on Topological Insulators." Lecture Notes in Physics 919 (2016)
5. T. Lepetit and B. Kanté, Phys. Rev. B - Condens. Matter Mater. Phys. 90, (2014).
6. T. Lepetit, E. Akmansoy, J. P. Ganne, and J. M. Lourtioz, Phys. Rev. B - Condens. Matter Mater. Phys. 82, (2010).